ACS APPLIED MATERIALS & INTERFACES

Research Article

Cite This: ACS Appl. Mater. Interfaces 2018, 10, 13479−13490

www.acsami.org

First-Principles Study of Lithium Cobalt Spinel Oxides: Correlating Structure and Electrochemistry

Soo Kim,[†,§] Vinay I. Hegde,[†] Zhenpeng Yao,[†] Zhi Lu,[†] Maximilian Amsler,[†,∥] Jiangang He,[†] Shiqiang Hao,[†] Jason R. Croy,[‡] Eungje Lee,*[,‡] Michael M. Thackeray,[‡] and Chris Wolverton*[,†]

[†]Department of Materials Science and Engineering, Northwestern University, 2220 Campus Drive, Evanston, Illinois 60208, United States

[‡]Chemical Sciences and Engineering Division, Argonne National Laboratory, 9700 S. Cass Avenue, Argonne, Illinois 60439, United States

Supporting Information

ABSTRACT: Embedding a lithiated cobalt oxide spinel ($Li_2Co_2O_4$, or $LiCoO_2$) component or a nickel-substituted $LiCo_{1-x}Ni_xO_2$ analogue in structurally integrated cathodes such as $xLi_2MnO_3{\cdot}(1-x)LiM'O_2$ (M′ = Ni/Co/Mn) has been recently proposed as an approach to advance the performance of lithium-ion batteries. Here, we first revisit the phase stability and electrochemical performance of $LiCoO_2$ synthesized at different temperatures using density functional theory calculations. Consistent with previous studies, we find that the occurrence of low- and high-temperature structures (i.e., cubic lithiated spinel LT-$LiCoO_2$; or $Li_2Co_2O_4$ ($Fd\bar{3}m$) vs trigonal-layered HT-$LiCoO_2$ ($R\bar{3}m$), respectively) can be explained by a small difference in the free energy between these two compounds. Additionally, the observed voltage profile of a Li/$LiCoO_2$ cell for both cubic and trigonal phases of $LiCoO_2$, as well as the migration barrier for lithium diffusion from an octahedral (O_h) site to a tetrahedral site (T_d) in $Fd\bar{3}m$ LT-$Li_{1-x}CoO_2$, has been calculated to help understand the complex electrochemical charge/discharge processes. A search of $LiCo_xM_{1-x}O_2$ lithiated spinel (M = Ni or Mn) structures and compositions is conducted to extend the exploration of the chemical space of Li−Co−Mn−Ni−O electrode materials. We predict a new lithiated spinel material, $LiNi_{0.8125}Co_{0.1875}O_2$ ($Fd\bar{3}m$), with a composition close to that of commercial, layered $LiNi_{0.8}Co_{0.15}Al_{0.05}O_2$, which may have the potential for exploitation in structurally integrated, layered spinel cathodes for next-generation lithium-ion batteries.

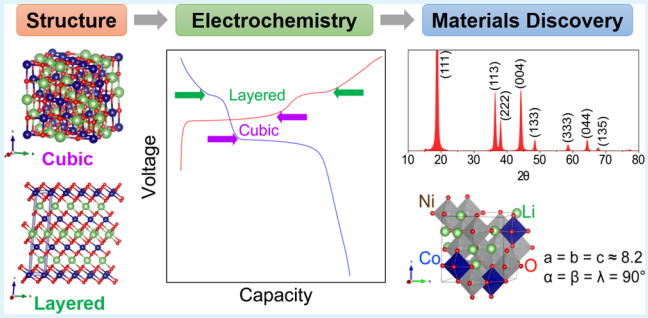

KEYWORDS: *lithium-ion battery, lithium cobalt oxide, overlithiated spinel, overpotential, migration barrier, structural search, materials discovery*

I. INTRODUCTION

In 1991, Sony introduced the first commercial lithium-ion battery (LIB), with carbon serving as the anode and a layered lithium cobalt oxide ($LiCoO_2$) as the cathode. Today, $LiCoO_2$ is still the predominant cathode material used in LIB products that power portable electronic devices. $LiCoO_2$ (LCO) has been synthesized both as a layered $R\bar{3}m$ structure (HT-LCO) at high temperatures (~900 °C) and as a cubic $Fd\bar{3}m$ structure (LT-LCO) at lower temperature (~400 °C).[1−13] Nearly 2 decades ago, Wolverton and Zunger demonstrated, using the first-principles full-potential linearized augmented planewave (FP-LAPW) method within the local density approximation (LDA), that the T = 0 K ground state structure of $LiCoO_2$ is the layered $R\bar{3}m$ structure (i.e., HT-LCO),[2] but the calculated energy difference between the layered and cubic structures of $LiCoO_2$ is very small (~0.01 eV/formula unit (fu)).[2,3] There have been substantial efforts to further investigate the thermodynamic phase stability of the Li_xCoO_2 system (for HT-LCO) using density functional theory (DFT) calculations within LDA[4−6] to explain the experimentally observed phase transformations during redox reactions of Li_xCoO_2 ($0 \le x \le 1$) electrodes. Early theoretical studies predicted that the composition $Li_{0.5}CoO_2$ energetically prefers the spinel structure over a layered structure,[3,7] and there is a thermodynamic driving force for the transformation of the layered compounds to a spinel (near x = 0.5) during electrochemical reactions. This prediction[3,7] was subsequently verified by transmission electron microscopy studies of HT-LCO electrodes that were subjected to extensive cycling.[8,9] Furthermore, Choi et al.[10] have shown that a $LiCo_2O_4$ spinel structure can be also synthesized by chemically extracting lithium from LT-$LiCoO_2$ (i.e., $Fd\bar{3}m$ LT-LCO; or $Li_2Co_2O_4$) at room temperature and have tested the

Received: January 8, 2018
Accepted: April 4, 2018
Published: April 4, 2018

DOI: 10.1021/acsami.8b00394
ACS Appl. Mater. Interfaces 2018, 10, 13479−13490

electrochemical profile of both LT- and HT-LCO cathode materials.

These early pioneering studies[1−13] opened up an opportunity to better understand the $LiCoO_2$ phase stability, particularly by focusing on the electrochemical performance of $LiCoO_2$ cathodes over long-term cycling. However, there have been long-standing discrepancies between the DFT calculated and experimental properties of $R\bar{3}m$ Li_xCoO_2 system cathodes, e.g., structural lattice parameters upon delithiation and average voltage. These discrepancies have been significantly clarified in a recent computational study,[14] where the inclusion of van der Waals (vdW) interactions in DFT calculations helped account for the weak dispersion forces that bind the layers, especially for the delithiated phase of $R\bar{3}m$ Li_xCoO_2 cathode materials.

In a recent experimental study, Long et al. suggested that embedding a small amount of a cobalt-containing spinel component in structurally integrated "layered−layered-spinel" (LLS) electrode materials might significantly enhance their electrochemical properties.[15] This study prompted a reinvestigation of lithiated spinel LT-$LiCoO_2$ (or, $Li_2Co_2O_4$) and LT-$LiCo_{1-x}Ni_xO_2$ ($0 < x \leq 0.2$) systems by Lee et al.,[16] with the argument that a lithiated cobalt oxide spinel component in a LLS electrode would be more beneficial than a manganese oxide spinel in terms of both delivered voltage and cycling stability—i.e., ∼3.6 V vs Li/Li^+ for $Li_{1-x}CoO_2$ ($0 \leq x \leq 0.5$) compared with ∼2.9 V for $Li_2Mn_2O_4$ and the lower mobility of cobalt ions relative to manganese ions in a close-packed oxygen array, respectively.[16]

Here, we revisit the phase stability of a cubic ($Fd\bar{3}m$) lithiated spinel $LiCoO_2$ structure (i.e., LT-LCO; or $Li_2Co_2O_4$) and a trigonal ($R\bar{3}m$) layered $LiCoO_2$ (i.e., HT-LCO) using first-principles calculations within the generalized gradient approximation (GGA) with the Hubbard U correction (GGA + U) scheme, as well as by employing vdW-inclusive functionals when necessary. Our findings can be summarized as follows: (i) a very small free energy difference between the cubic $Fd\bar{3}m$ spinel (LT-LCO) phase and the trigonal $R\bar{3}m$ layered (HT-LCO) phase explains the coexistence of both phases in ref 16 at low/moderate temperatures, (ii) a favorable lithium ion migration from an octahedral to a tetrahedral site occurs in LT-LCO during electrochemical charging, confirmed by both DFT and ex situ X-ray diffraction (XRD) analysis, and (iii) a structural search within Li−Co−Mn−Ni−O chemical space predicts a possible $LiCo_{0.1875}Ni_{0.8125}O_2$, overlithiated spinel oxide. Our DFT study provides an opportunity to understand and improve the existing LIB technology by exploiting cobalt- and nickel-based spinel oxide materials in structurally integrated, layered spinel electrodes.

II. METHODS

All the DFT calculations were carried out within the Vienna ab initio simulation package using projected augmented wave pseudopotentials and the Perdew−Burke−Ernzerhof (PBE) exchange−correlation functional of the generalized gradient approximation (GGA).[17−19] We used Dudarev's rotationally invariant DFT + U approach to treat the 3d electrons of Co, Mn, and Ni ions.[20] The U values of 3.3, 3.8, and 6.4 eV were used for Co, Mn, and Ni, respectively. The Heyd−Scuseria−Ernzerhof (HSE) screened hybrid density functional HSE06 calculations[21,22] were also performed for a comparison with GGA + U voltages (see Section II.II and Table 2). We used a cutoff energy of 520 eV for the planewave basis set in all the calculations. We used k-point meshes up to 8000 k-points per reciprocal atom (KPPRA) to obtain accurate total DFT energies (∼4000 KPPRA for HSE calculations). Unless noted, all the atomic positions were relaxed with symmetry-broken DFT calculations to fully capture the local variations of Li−O, Co−O, and Ni−O polyhedral clusters. VESTA[23] was used to visualize the crystal structures.

II.I. Structure Prediction and Free Energy. Structure prediction calculations were performed using the minima hopping method (MHM)[24,25] to explore the ground state and other low-energy polymorphs of $LiCoO_2$. The MHM implements a reliable algorithm to explore the potential energy surface by efficiently sampling the low-lying local minima using consecutive, short molecular dynamics (MD) escape steps followed by local geometry optimizations.[26−29] The Bell−Evans−Polanyi principle is exploited by aligning the initial MD velocities along the soft-mode directions to accelerate the search.[30,31] The vibrational entropy and Helmholtz free energy of the $Fd\bar{3}m$ and $R\bar{3}m$ structures were calculated with the PHONOPY code[32] within the harmonic approximation.

II.II. Delithiation. A previous DFT study by Aykol et al.[14] suggested that initializing DFT calculation with different magnetic moments (0−5 μ_B for Co) can result in energies up to ∼130 meV/atom higher than the ground state due to the existence of both low- and high-spin states of Co. It was also determined that assigning low-spin Co^{3+} ($t_{2g}^6e_g^0$) with no magnetic moment (0 μ_B) and low-spin Co^{4+} ($t_{2g}^5e_g^0$) with a magnetic moment of 1 μ_B results in the lowest-energy solution for $Li_{0.5}CoO_2$ with an U_{Co} value of 3.3 eV.[14] Consistent with a previous study,[14] we observe that assigning moments of 0 and 1 μ_B to Co^{3+} and Co^{4+}, respectively, usually resulted in the low-energy solutions (by up to ∼30 meV/atom) after being allowed to relax to self-consistency during DFT calculation. We also find that the "final" resulting magnetic moments always end up being close to the assigned "initial" magnetic moments, e.g., ∼0 and ∼1 μ_B for Co^{3+} and Co^{4+}, respectively, for a number of Li_xCoO_2 systems tested in the current work. For calculation of energetics during the delithiation process, we treat the Co closest to a lithium vacancy to be 4+, and we confirmed that this indeed results in energetically more favorable solutions, up to ∼5 meV/atom lower in energy than any other possible arrangement. We considered $Fd\bar{3}m$ LT-LCO supercells consisting of 16 fu for all our delithiation calculations. The unique Li sites within the supercells were identified using symmetry-determining algorithms implemented in the Materials INTerface suite (MINT) package, freely available for download at https://github.com/materials/mint.[33] We removed the most weakly bound Li atom at each composition, starting from $Li_{16}Co_{16}O_{32}$ to $Li_8Co_{16}O_{32}$ (i.e., carrying out a dilute limit voltage calculation). We calculated the energy difference between overlithiated $Li_{16}Co_{16}O_{32}$ spinel (all the lithium ions in the octahedral sites) and $Li_8Co_{16}O_{32}$ spinel (all the lithium ions in the tetrahedral sites) to obtain the average voltage of the two-phase reaction: $2LiCoO_2 \rightarrow LiCo_2O_4 + Li^+ + e^-$. We monitored the changes in the cathode structure (i.e., lattice parameters) and its oxidation states (i.e., Bader charge analysis) in all the DFT calculations.

II.III. Li^+ Migration in $Fd\bar{3}m$ LT-LCO. The climbing image nudged elastic band (ci-NEB) method[34,35] was used to find the minimum energy barrier between the octahedral (O_h) and tetrahedral (T_d) Li^+ sites in $Fd\bar{3}m$ $Li_{1-x}CoO_2$ structures in the compositions of $Li_{10}Co_{16}O_{32}$ and $Li_8Co_{16}O_{32}$. These two compositions, close to $LiCo_2O_4$ spinel (i.e., all the Li atoms occupying T_d sites), were chosen to investigate the energetic landscape of lithium migrations from O_h to T_d in the $Fd\bar{3}m$ $Li_{1-x}CoO_2$ systems.

II.IV. Ex Situ X-ray Diffraction. The preparation of LT-$LiCo_{0.9}Ni_{0.1}O_2$ cathode materials is described elsewhere.[16] Ex situ X-ray diffraction (XRD) analysis of the cycled electrodes collected at different states of charge/discharge was carried out at beamline 11-BM of the Advanced Photon Source in the Argonne National Laboratory to investigate the Li^+ ion migration tendencies ($O_h \leftrightarrow T_d$) in the LT-phase.

II.V. Structural Search. We used the structure generating algorithms implemented in the Enum package[36−38] to construct possible mixing configurations of transition metal (TM) atoms in the cubic $Fd\bar{3}m$ and layered $R\bar{3}m$ $Li_{16}Co_{16-x}M_xO_{32}$ structures (up to 64 total atoms in the supercell; M = Ni or Mn; $0 \leq x \leq 16$)—a total of 531 structures for $Fd\bar{3}m$ and 2250 structures for $R\bar{3}m$. We calculated

DOI: 10.1021/acsami.8b00394
ACS Appl. Mater. Interfaces 2018, 10, 13479−13490

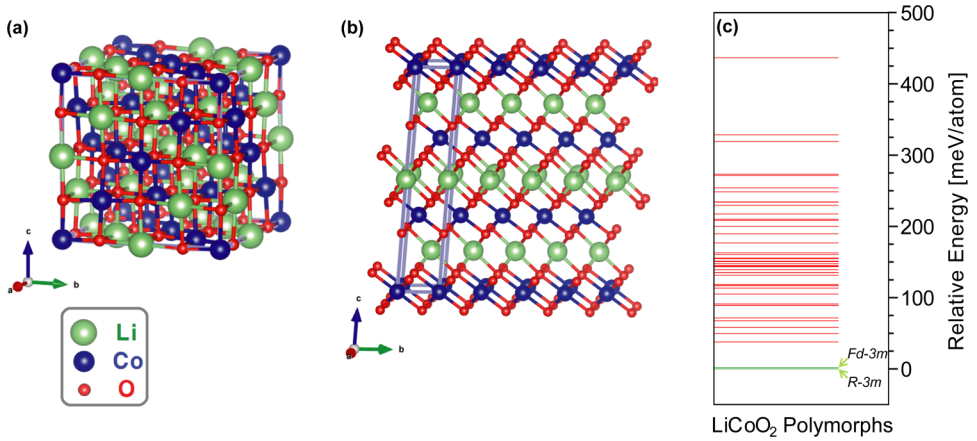

Figure 1. Crystal structures of (a) $Fd\bar{3}m$ spinel $LiCoO_2$ (LT-LCO; or $Li_2Co_2O_4$) and (b) $R\bar{3}m$ layered $LiCoO_2$ (HT-LCO). (c) The relative energy scale of $LiCoO_2$ polymorphs (calculated within GGA + U), where all the $LiCoO_2$ crystal structures are generated using the minima hopping method (MHM).[24,25] Crystal structure prediction using MHM runs confirms that both $Fd\bar{3}m$ and $R\bar{3}m$ $LiCoO_2$ phases are indeed the two lowest energy $LiCoO_2$ polymorphs with a significant energy gap to the next higher energy polymorph.

the electrostatic energies of all such structures using MINT,[33] and further calculated the three structures with the lowest electrostatic energy at each composition within the previously described DFT formalism using GGA + U. Furthermore, all the ground state phases available in the chemical space of Li−Co−Mn−Ni−O (i.e., reference chemical potentials) in the Open Quantum Materials Database (OQMD)[39,40] were recalculated with consistent DFT settings. In addition, we included "normal" $Li(Co_{1-x}M_x)_2O_4$ spinel oxides (M = Mn and Co; $0 \le x \le 1$), $LiNi_{0.5}Mn_{1.5}O_4$, $LiNiMnO_4$, $LiNi_{0.333}Co_{0.333}Mn_{0.333}O_2$, $LiCo_{0.67}Mn_{0.33}O_2$, $LiCo_{0.17}Ni_{0.83}O_2$, $LiMn_{0.5}Ni_{0.5}O_2$, $LiMn_{0.33}Ni_{0.66}O_2$, $LiMn_{0.14}Ni_{0.86}O_2$, $Li(Ni_{0.31}Co_{0.19}Mn_{0.5})_2O_4$, and $Li(Co_{0.31}Ni_{0.19}Mn_{0.5})_2O_4$ phases for the thermodynamic stability assessment in the Li−Co−Mn−Ni−O system.

III. RESULTS AND DISCUSSION

III.I. Structure. *III.I.I. LT- and HT-LCO.* Figure 1a,b show the relaxed structures of $Fd\bar{3}m$ $LiCoO_2$ cubic spinel (LT-LCO; or $Li_2Co_2O_4$) and $R\bar{3}m$ layered $LiCoO_2$ (HT-LCO) from GGA + U calculations. The lattice parameters determined from GGA + U scheme are provided in Table 1. In a previous study by Lee et al.,[16] a sample of $LiCoO_2$ powder prepared at 400 °C for 6 days (denoted as "LT-phase") was analyzed using high-resolution synchrotron X-ray diffraction and high-resolution transmission electron microscopy. Their results suggested that the LT-phase powder contains both $Fd\bar{3}m$ and $R\bar{3}m$ $LiCoO_2$ structures. We believe that the synthesis of $Fd\bar{3}m$ LT-LCO (or LT-phase consisting both $Fd\bar{3}m$ and $R\bar{3}m$) at low temperatures[16] is due to sluggish kinetics, whereas at high heat-treatment temperatures, fast kinetics enable the system to reach thermodynamic equilibrium to form the layered structure (HT-LCO).[3] In other words, the very small difference in the energies of the competing polymorphs (Table 1), at least in part, can explain the coexistence of both $Fd\bar{3}m$ and $R\bar{3}m$ phases in the LT-phase powders prepared in ref 16.

Table 1. Structural Properties of LT-LCO and HT-LCO Obtained from GGA + U Calculations[a]

structure	space group	a (Å)	c (Å)	c/a	$E_{0,GGA+U}$ (eV/fu)
LT-LCO	$Fd\bar{3}m$	8.0644 ($a = b = c$)	n/a	n/a	−22.740
HT-LCO	$R\bar{3}m$	2.8398	14.1473	4.98	−22.748

[a]The space group after the relaxation is identified with MINT.[33] We observe a very small difference in the calculated energies between $Fd\bar{3}m$ spinel $LiCoO_2$ (i.e., LT-LCO; or $Li_2Co_2O_4$) and $R\bar{3}m$ layered $LiCoO_2$ (HT-LCO).

Wolverton and Zunger previously reported that the calculated energy difference between $Fd\bar{3}m$ spinel $LiCoO_2$ (LT-LCO; or $Li_2Co_2O_4$) and $R\bar{3}m$ layered $LiCoO_2$ (HT-LCO) is very small (i.e., ∼2 meV/atom; or ∼8 meV/fu) within the DFT calculations based on LDA and FP-LAPW.[2,3] In this current work, our GGA + U results agree with these previous calculations with a high degree of quantitative precision, even though the DFT method is different (i.e., FP-LAPW vs planewave) and the exchange−correlation functional is different (i.e., LDA vs PBE). Here, we consistently find that the energy difference between the layered and cubic $LiCoO_2$ is very small at ∼2 meV/atom (without vdW corrections), where the layered $LiCoO_2$ is lower in energy.

We performed additional DFT calculations incorporating opt-type (optPBE) van der Waals density functionals (vdW-DF)[14,41−43] to both $Fd\bar{3}m$ and $R\bar{3}m$ $LiCoO_2$ structures; also, we find that the energy difference between the two phases is not significantly affected by including the vdW-DF. Previous studies[14] have shown that vdW corrections are essential for accurately predicting the structural properties (e.g., lattice parameters, interlayer spacing, and crystal volume) of $R\bar{3}m$ Li_xCoO_2 at $x < 0.5$; however, at $x = 1$, for the fully lithiated $R\bar{3}m$ $LiCoO_2$, these structural properties were only slightly improved by accounting for dispersion interactions. Overall, our theoretical study confirms that the layered compound is always lower in energy regardless of the inclusion of vdW correction. This finding is also consistent with the earlier experimental result suggesting that the lithiated spinel synthesized at low temperatures slowly transforms to a more thermodynamically stable layered $LiCoO_2$.[44]

Lastly, to ensure that $Fd\bar{3}m$ and $R\bar{3}m$ $LiCoO_2$ phases are energetically the most stable structures at the composition, we used the MHM[24,25] to survey the potential energy landscape of $LiCoO_2$ (up to 16 atoms per supercell). Here, we used both $Fd\bar{3}m$ and $R\bar{3}m$ $LiCoO_2$ phases as the seed structures for the MHM runs. As shown in Figure 1c, $Fd\bar{3}m$ and $R\bar{3}m$ $LiCoO_2$ phases are indeed the two lowest-energy polymorphs among the 122 unique configurations sampled, where the MHM did not find any other structure lower in energy. The structure next

DOI: 10.1021/acsami.8b00394
ACS Appl. Mater. Interfaces 2018, 10, 13479−13490

lowest in energy belongs to a hexagonal space group ($P\bar{3}m1$) with an ABAB stacking sequence; however, it is ~35 meV/atom higher in energy than the $Fd\bar{3}m$ and $R\bar{3}m$ polymorphs.

III.I.II. Free Energy of $LiCoO_2$. So far, we have only described the 0 K energetics of the relevant phases. Because the $R\bar{3}m$ and $Fd\bar{3}m$ structures are energetically nearly degenerate, the entropy may significantly affect the stability of the $Fd\bar{3}m$ and $R\bar{3}m$ $LiCoO_2$ structures at finite temperatures.[45] Because both $Fd\bar{3}m$ and $R\bar{3}m$ $LiCoO_2$ structures are ordered, the free energy (F) then can be calculated by including the vibrational entropy: $F = E_0 - TS_{vib}$, where E_0, S_{vib}, and T are the internal DFT energy of $LiCoO_2$ determined within GGA + U, the vibrational entropy (GGA + U calculated), and temperature, respectively. Figure 2 shows the difference in the free energy between $Fd\bar{3}m$ LT-LCO and $R\bar{3}m$ HT-LCO, which is extremely competitive between 0 and 1500 K. However, Figure 2 also shows that HT-LCO is the ground state structure of $LiCoO_2$ system at all the temperatures. We tested the above behavior of free energy with temperature using opt-type vdW corrections;[14,41−43] however, they did not affect the main conclusion that $R\bar{3}m$ HT-LCO is always more stable than $Fd\bar{3}m$ LT-LCO at all the temperatures. Because the difference in free energies of the two phases is very small at all the temperatures, it suggests that the $Fd\bar{3}m$ $LiCoO_2$ (or $Li_2Co_2O_4$) phase can be formed at low and medium temperatures. At higher temperatures, we expect the system to find the equilibrium state (where kinetics are also faster) to observe the $R\bar{3}m$ HT-LCO phase. In conclusion, our theoretical calculations are consistent with the previous experimental observations (and previous calculations).[1−3,8−13,44] We further discuss the stability of the $Fd\bar{3}m$ phase with Ni substitution[16] in the Supporting Information (SI, Section S1).

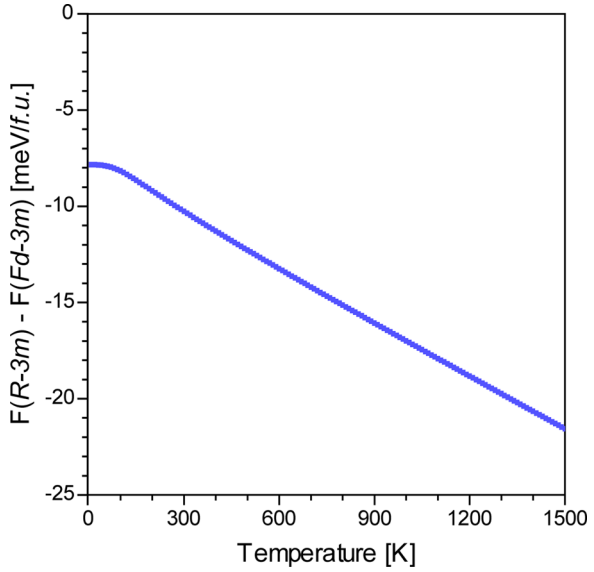

Figure 2. Calculated free energy difference between $R\bar{3}m$ and $Fd\bar{3}m$ $LiCoO_2$, suggesting that the $R\bar{3}m$ structure becomes increasingly more stable than $Fd\bar{3}m$ $LiCoO_2$ (or $Li_2Co_2O_4$) at higher temperatures.

III.II. Electrochemical Properties of LT-LCO and HT-LCO. *III.II.I. Layered vs Cubic DFT Voltages.* Figure 3a shows a conventional $Fd\bar{3}m$ $LiCoO_2$ supercell consisting of 16 fu; and Figure 3b shows $Li_{0.5}CoO_2$ (or $LiCo_2O_4$ spinel) all Li^+ ions occupying the tetrahedral 8a sites. The layered $R\bar{3}m$ $LiCoO_2$ structure is shown in Figure 1b. The calculated GGA + U (U_{Co} = 3.3 eV) voltages of $R\bar{3}m$ HT-LCO and $Fd\bar{3}m$ LT-LCO charged to $Li_{0.5}CoO_2$ are found to be 3.58 and 3.31 V (vs Li/Li^+), respectively. In addition, Table 2 provides a summary of the DFT (and HSE) calculated voltages of $R\bar{3}m$ and $Fd\bar{3}m$ $LiCoO_2$ charged to $Li_{0.5}CoO_2$ and CoO_2 and the comparison with experiments.[3,14,11,16,46] We observe that the most accurate voltage of $R\bar{3}m$ $LiCoO_2$ cathodes can be predicted when using the opt-type vdW corrections.[14,41−43] In the case of $Fd\bar{3}m$ $LiCoO_2$ cathode, both LDA[3] and GGA + U (U_{Co} = 5 eV) scheme can closely predict the experimental voltages.[11,16,46] The HSE06 results slightly overestimate the experimental voltages in all the cases. The experimental charge/discharge voltage vs capacity curves of synthesized $LiCoO_2$ powders at 400 °C in ref 16 are provided in Figure 4, reported to contain both $Fd\bar{3}m$ and $R\bar{3}m$ phases within a single-powder sample.

As seen from Table 2, our GGA (with or without +U and/or vdW correction) and HSE06 calculation results indicate that Li^+ ion extraction from the octahedral (O_h) sites of $Fd\bar{3}m$ LT-LCO (Figure 3a) resulting in $Fd\bar{3}m$ $LiCo_2O_4$ spinel shown in Figure 3b (i.e., structure with all the Li^+ ion migrated from O_h to T_d; $Fd\bar{3}m$ $LiCoO_2$ → $Fd\bar{3}m$ $Li_{0.5}CoO_2$) occurs at a lower voltage than Li^+ ion extractions from the layered $R\bar{3}m$ HT-LCO (shown in Figure 1b), in good agreement with the electrochemistry data shown in Figure 4. We note that the extraction of Li^+ ion from a tetrahedral (T_d) site of $LiCo_2O_4$ (Figure 3b) toward $Li_{1-x}Co_2O_4$ occurs at a voltage ~0.9 V higher than that for Li^+ extraction from O_h sites.[16] We further discuss the mechanisms of Li^+ ion extraction by constructing a LT-/HT-LCO interface model in the SI (Section S2).

III.II.II. Delithiation of $Fd\bar{3}m$ LT-LCO and Li^+ Migration Kinetics. In Figure 4, we observe a voltage hysteresis at 3.7 V (charging) and 3.5 V (discharging) for the $Fd\bar{3}m$ LT-LCO component but not for the $R\bar{3}m$ HT-LCO component (i.e., both charging and discharging plateaus can be found at 3.9 V).

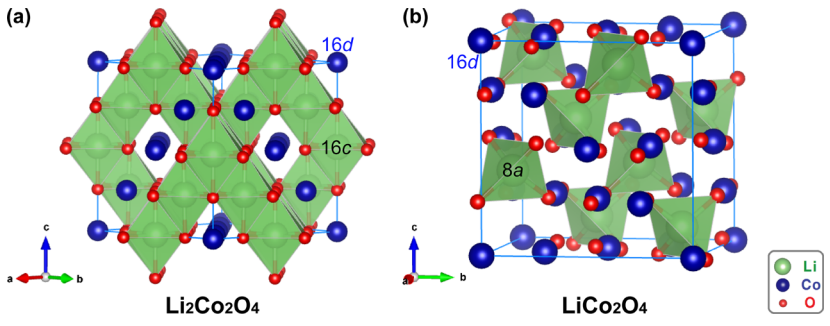

Figure 3. Crystal structures of (a) overlithiated $Fd\bar{3}m$ LT-$LiCoO_2$ (or $Li_2Co_2O_4$) and (b) spinel $Fd\bar{3}m$ $Li_{0.5}CoO_2$ ($LiCo_2O_4$ normal spinel). Lithium ions occupy 16c octahedral sites and 8a tetrahedral sites in $Li_2Co_2O_4$ (panel a) and $LiCo_2O_4$ (panel b), respectively.

DOI: 10.1021/acsami.8b00394
ACS Appl. Mater. Interfaces 2018, 10, 13479−13490

Table 2. Summary of the Calculated vs Experimental Voltages of LT-LCO ($Fd\bar{3}m$) and HT-LCO ($R\bar{3}m$) from $LiCoO_2$ → $Li_{0.5}CoO_2$ (Li_1 to $Li_{0.5}$) and $LiCoO_2$ → CoO_2 (Li_1 to Li_0)

voltage (V vs Li/Li^+)	$Fd\bar{3}m$ (Li_1 to $Li_{0.5}$)	$Fd\bar{3}m$ (Li_1 to Li_0)	$R\bar{3}m$ (Li_1 to $Li_{0.5}$)	$R\bar{3}m$ (Li_1 to Li_0)
LDA[3]	3.50	3.91	3.37	3.78
GGA[a,14]	2.61	3.41	3.0	3.3
GGA + U (U_{Co} = 3.3 eV)[a]	3.31	3.89	3.58	3.80
GGA + U (U_{Co} = 5 eV)[a,14]	3.41	4.02	3.6	3.8
optPBE + U (U_{Co} = 4 eV)[a,14]	3.16	3.71	3.9	4.1
HSE06[a,14]	3.95	4.66	4.2	4.5
charge (exp.)[11,16,46]	3.7	≥4.3	3.9	4.1
discharge (exp.)[11,16,46]	3.3	~3.6	3.9	3.8

[a]This work.

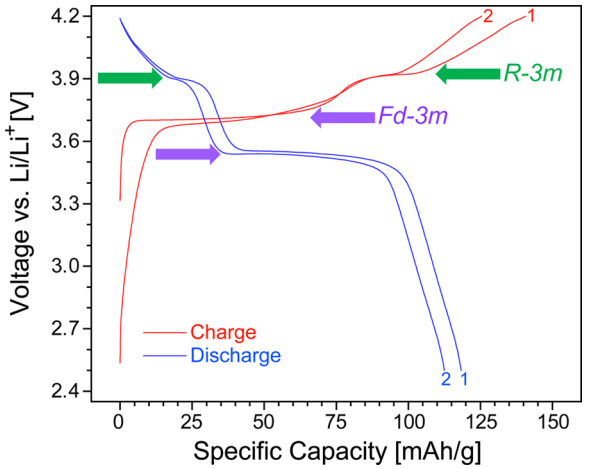

Figure 4. Experimental voltage vs capacity curves for $LiCoO_2$ synthesized at 400 °C composed of both $Fd\bar{3}m$ and $R\bar{3}m$ phases. First, we observe the charging and discharging plateaus of $Fd\bar{3}m$ phase at 3.7 and 3.5 V, respectively (indicated by the purple arrows). The redox reaction of $R\bar{3}m$ phase occurs at 3.9 V (indicated by the green arrows). Adapted with permission from ref 16. Copyright 2017 American Chemical Society.

As mentioned in Section III.II.I, the calculated DFT voltage between LT-LCO ($Li_2Co_2O_4$) and $LiCo_2O_4$ (also see Figure 5a,d), where lithium ions occupy all the octahedral (O_h) sites and tetrahedral (T_d) sites in $Li_2Co_2O_4$ and $LiCo_2O_4$, respectively, is 3.31 V. From here on, we will refer to this DFT voltage of 3.31 V as the "equilibrium DFT voltage" of the following charging reaction: $2Li_{(16c)}CoO_2 \rightarrow Li_{(8a)}Co_2O_4 + Li^+ + e^-$.

We carefully studied the preference of Li^+ ion occupations between O_h vs T_d sites during delithiation of the $Fd\bar{3}m$ LT-$LiCoO_2$ (or, $Li_2Co_2O_4$) cathode. While the M−O framework remains the same in the $Fd\bar{3}m$ LT-$LiCoO_2$ (or, $Li_2Co_2O_4$) and $LiCo_2O_4$ spinel structures, the occupancy of Li^+ ions changes from O_h to T_d sites during the charging process. Therefore, starting from the supercell shown in Figure 5a (i.e., $Li_{16}Co_{16}O_{32}$), the lowest energy lithium vacancies were successively created (i.e., by removing one Li at a time, and by testing all the Li positions for each cell to find the lowest-energy Li to be removed), until the composition of $Li_8Co_{16}O_{32}$ was reached (Figure 5c). From our calculations of the charging cycle, we find that lithium ion migration from an O_h site to an adjacent T_d site becomes energetically favorable (with no barrier) only at a composition of $Li_{11}Co_{16}O_{32}$ (i.e., with all the

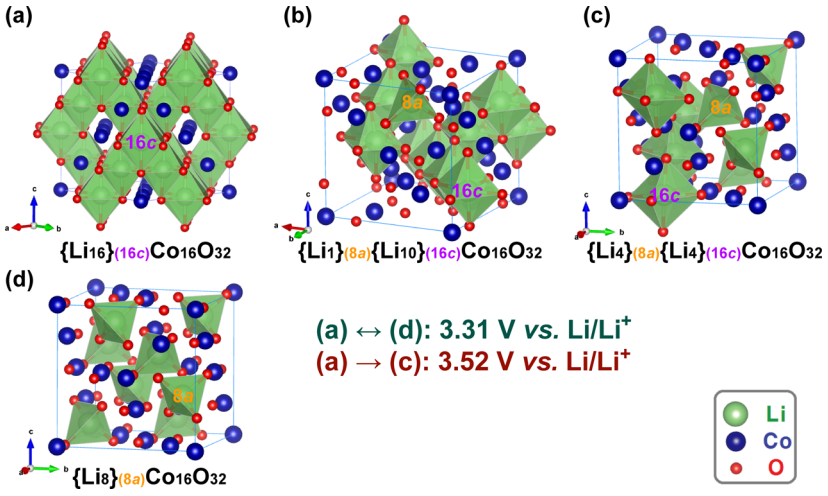

Figure 5. Crystal structures of (a) $Fd\bar{3}m$ LT-LCO $\{Li_{16}\}_{(16c)}Co_{16}O_{32}$, where Li^+ ions occupy all the 16c octahedral (O_h) sites, (b) $\{Li_1\}_{(8a)}\{Li_{10}\}_{(16c)}Co_{16}O_{32}$, where one Li^+ occupies an 8a tetrahedral (T_d) site, and all other Li^+ ions occupy the 16c octahedral sites, (c) $\{Li_4\}_{(8a)}\{Li_4\}_{(16c)}Co_{16}O_{32}$, where 50% of Li^+ ions occupy the T_d and the other 50% occupy the O_h, and (d) $Fd\bar{3}m$ normal $\{Li_8\}_{(8a)}Co_{16}O_{32}$ spinel, where Li^+ ions occupy all the 8a tetrahedral (T_d) sites. All of the other intermediate compositions between panel (a) and (c) (i.e., $Li_{15}Co_{16}O_{32}$, $Li_{14}Co_{16}O_{32}$, $Li_{13}Co_{16}O_{32}$, $Li_{12}Co_{16}O_{32}$, $Li_{10}Co_{16}O_{32}$, $Li_9Co_{16}O_{32}$) are not shown for purposes of brevity. Our DFT calculations indicate that the $\{Li_4\}_{(8a)}\{Li_4\}_{(16c)}Co_{16}O_{32}$ phase could result in an increased overpotential of ~0.2 V during the charging cycle of LT-LCO. However, other structural factors such as interfacial resistances and disorders in Li/TM layers may also contribute to the observed hysteresis.

DOI: 10.1021/acsami.8b00394
ACS Appl. Mater. Interfaces 2018, 10, 13479−13490

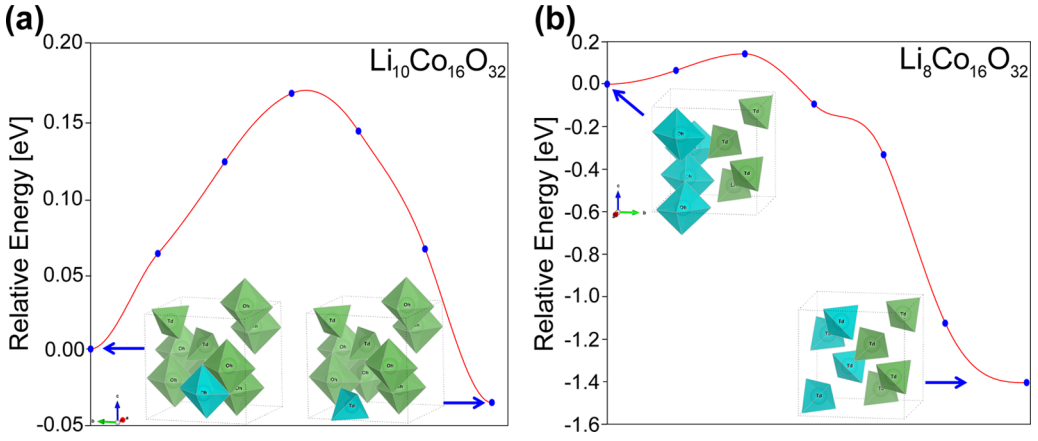

Figure 6. Barrier for Li^+ ion migration, calculated using the nudged elastic band (NEB) method energy barrier calculations of Li^+ ion migration in (a) $Li_{10}Co_{16}O_{32}$ and (b) $Li_8Co_{16}O_{32}$ (or $LiCo_2O_4$). Only Li−O polyhedral clusters are shown for clarity. For panel (b), we observe that all the Li atoms relax spontaneously into T_d sites, even if we only move one O_h Li into the adjacent T_d site.

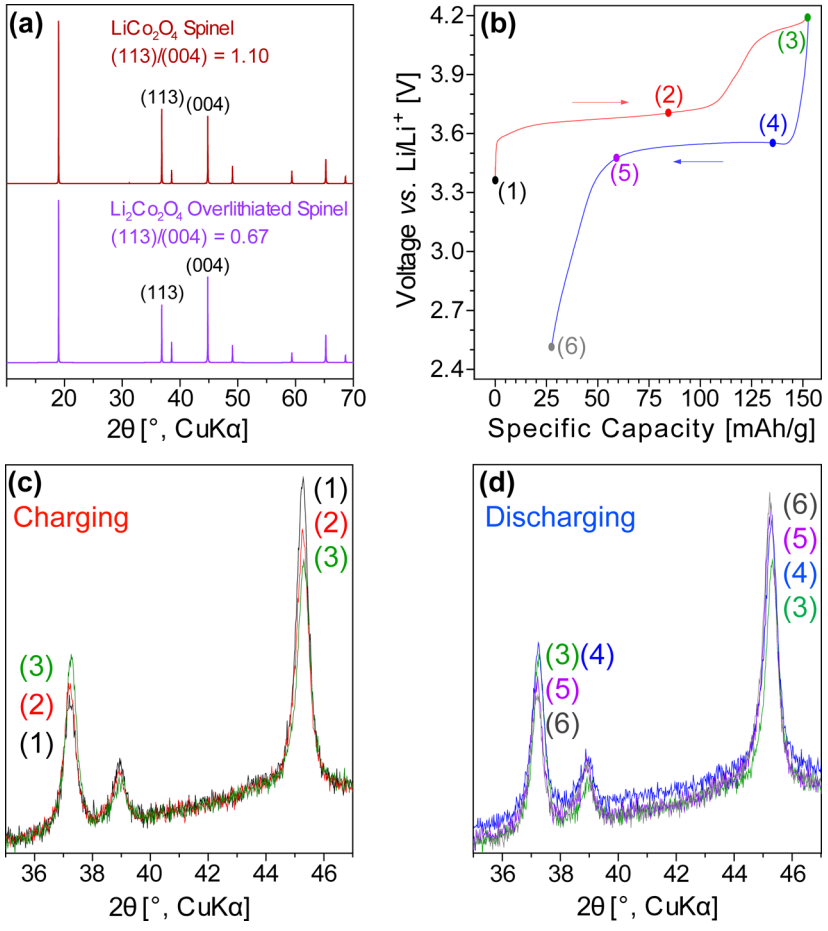

Figure 7. (a) Calculated X-ray diffraction (XRD) patterns of LT-$LiCoO_2$ (i.e., $Li_2Co_2O_4$) and $LiCo_2O_4$ spinel compounds. (b) Experimental voltage vs capacity curves for LT-$LiCo_{0.9}Ni_{0.1}O_2$ synthesized at 400 °C,[16] where the cathode sample is mainly composed of $Fd\bar{3}m$ LT-phase (please note that the layered phase still exists in the sample: see ref 16). The ex situ XRD patterns of LT-$LiCo_{0.9}Ni_{0.1}O_2$ during charging (panel c) and discharging (panel d) are shown. The XRD peak intensity ratios of $I_{(113)}/I_{(004)}$ during the charge/discharge runs (i.e., panels (c) and (d), respectively) are provided in Table 3.

other 10 lithium ions still occupying the O_h sites, as shown in Figure 5b). We repeated the above procedure (i.e., create the energetically most favorable lithium vacancy in the lowest-energy $Li_{16-x}Co_{16}O_{32}$ structure) and find a $Li_8Co_{16}O_{32}$ structure that contains 50% of lithium ions at T_d sites and the other 50% of lithium ions at O_h sites (Figure 5c). In other words, in each delithiation step from $Li_{11}Co_{16}O_{32}$ onward, one more of the remaining lithium atoms in the O_h sites migrates to an adjacent T_d site until the composition of $Li_8Co_{16}O_{32}$ is reached (shown in Figure 5c, with four Li^+ in T_d and four Li^+ in O_h). The difference between the energy of the ground state $Li_{(8a)}Co_2O_4$ spinel structure with all lithium atoms occupying

DOI: 10.1021/acsami.8b00394
ACS Appl. Mater. Interfaces 2018, 10, 13479−13490

8a T_d sites (Figure 5d; $\{Li_8\}_{(8a)}Co_{16}O_{32}$) and the $\{Li_{0.5}\}_{(8a)}\{Li_{0.5}\}_{(16c)}Co_2O_4$ structure (Figure 5c; $\{Li_4\}_{(8a)}\{Li_4\}_{(16c)}Co_{16}O_{32}$) is ~33 meV/atom. The calculated DFT voltage between $Li_{(16c)}CoO_2$ in Figure 5a (i.e., $\{Li_{16}\}_{(16c)}Co_{16}O_{32}$) and $\{Li_{0.5}\}_{(8a)}\{Li_{0.5}\}_{(16c)}Co_2O_4$ in Figure 5c (i.e., $\{Li_4\}_{(8a)}\{Li_4\}_{(16c)}Co_{16}O$) is 3.54 V (that is, ~0.2 V higher than the equilibrium DFT voltage; please refer to refs 47−49 for the rationale behind using the metastable phase on the (de-)lithiation reactions). We note that phases other than the lowest-energy ones that we report in this work could be further computed to identify a number of metastable phases at each composition, but it is likely that such higher-energy metastable phases would only increase the voltage hysteresis beyond 0.2 V. Thus, we believe that the formation of the metastable $\{Li_{0.5}\}_{(8a)}\{Li_{0.5}\}_{(16c)}Co_2O_4$ phase shown in Figure 5c could directly contribute to an increased overpotential of ~0.2 V during the charging cycle of $Fd\bar{3}m$ LT-LCO component (see Figure 4); however, it is also possible that other complexities present within the composite cathodes such as intergrown layered/spinel domains and/or residual TM ions in the lithium layer[16] also play important roles in impeding lithium ion kinetics in the system. The existence of metastable phases during charging cycles has been previously observed in a number of systems in both experimental and theoretical studies.[50−53] During the discharge cycles, on the other hand, a sufficient number of lower-energy vacant O_h sites are available, where lithium ions can be inserted. The discharge process may then follow the "equilibrium" reaction pathway (i.e., $Li_{(8a)}Co_2O_4 + Li^+ + e^- \rightarrow 2Li_{(16c)}CoO_2$).

For selected $Fd\bar{3}m$ $Li_{1-x}CoO_2$ structures, we investigated the energy barrier for Li^+ ion migration using the ci-NEB method, where we displaced one Li atom from an O_h site to an adjacent T_d site. Figure 6 shows the calculated NEB energy barriers for Li^+ migration at compositions of $Li_{10}Co_{16}O_{32}$ and $Li_8Co_{16}O_{32}$. The barrier for Li^+ migration is found to be small in both structures (~0.15 eV). However, the relative energy difference before and after Li^+ ion migration (or the "thermodynamic driving force") in $Li_8Co_{16}O_{32}$ is calculated to be much larger than that in $Li_{10}Co_{16}O_{32}$ (−0.175 vs −0.003 eV/Li^+). In fact, once one of the Li^+ in the O_h site migrates to an adjacent T_d site in the metastable $Li_8Co_{16}O_{32}$ structure (found in Figure 5c), all the remaining Li^+ ions in O_h sites migrate to the adjacent T_d sites, as shown in Figure 6b. In the subsequent section, we will monitor the Li^+ ion migration (O_h vs T_d) as a function of state-of-charge via ex situ X-ray diffraction analysis to further understand the Li^+ migration kinetics in $Fd\bar{3}m$ $Li_{1-x}CoO_2$.

III.II.III. Ex Situ X-ray Diffraction Analysis on $Fd\bar{3}m$ LT-$LiCo_{0.9}Ni_{0.1}O_2$. In this section, we monitor the evolution of the X-ray diffraction (XRD) pattern of a LT-$LiCo_{0.9}Ni_{0.1}O_2$ cathode during the first charge/discharge cycling. Because the prepared sample (LT-$LiCo_{0.9}Ni_{0.1}O_2$) has a predominantly lithiated spinel character (see ref 16), we choose this as a model system to investigate the Li^+ migration tendencies in the $Fd\bar{3}m$ phase of $LiCoO_2$ (or $Li_2Co_2O_4$). Figure 7a shows the simulated XRD patterns of $Fd\bar{3}m$ overlithiated $LiCoO_2$ spinel (i.e., $Li_2Co_2O_4$) and $Fd\bar{3}m$ $LiCo_2O_4$ spinel oxide. We observe that the simulated XRD patterns are quite similar to each other, except that the peak intensity ratio of $I_{(113)}/I_{(004)}$ can help distinguish the structural differences between the two cubic structures (i.e., lithium ions occupying 16c O_h and 8a T_d sites in $Li_2Co_2O_4$ and $LiCo_2O_4$, respectively; see Section S3 in the SI for further discussions). Figure 7b shows the electrochemical profiles for the first cycle of Li/LT-$LiCo_{0.9}Ni_{0.1}O_2$ cell, where we collect the XRD patterns at various states-of-charge (see Figure 7c,d). The ratios of $I_{(113)}/I_{(004)}$ XRD peak intensities for various potentials of Li/LT-$LiCo_{0.9}Ni_{0.1}O_2$ cell are summarized in Table 3. From

Table 3. XRD Peak Intensity Ratio of $I_{(113)}/I_{(004)}$ at Various State of Charge of $LiNi_{0.1}Co_{0.9}O_2$ Cathode Materials, Mainly Composed of $Fd\bar{3}m$ Phase[a,16]

state-of-charge in Figure 7b	(1)	(2)	(3)	(4)	(5)	(6)
x in $Li_{1-x}MO_2$	0	0.30	0.55	0.49	0.21	0.10
$I_{(113)}/I_{(004)}$	0.44	0.53	0.75	0.64	0.51	0.45

[a]The higher values of $I_{(113)}/I_{(004)}$ directly indicate that more lithium ions are occupying the T_d sites of $Fd\bar{3}m$ phase (i.e., $I_{(113)}/I_{(004)} = 1.1$). The lower values of $I_{(113)}/I_{(004)}$ indicate that more lithium ions are occupying the O_h sites (see Figure 7a). For further discussions, please see Section S3 in the SI.

our results, we can observe that the $I_{(113)}/I_{(004)}$ ratio is almost the same at the beginning and at the end of the charge/discharge runs, at (1) and (6), respectively. More interestingly, the $I_{(113)}/I_{(004)}$ ratio is found to be very close to each other at (2) and (5). At point (2), the majority of lithium ions occupying the 16c O_h sites of $Fd\bar{3}m$ $Li_{2-x}Co_2O_4$ phase should already be extracted from the cathode materials. At point (5), most of the lithium ions are being inserted back to the O_h sites in the $Fd\bar{3}m$ phase. This qualitatively implies that many remaining lithium ions in the $Fd\bar{3}m$ phase are still occupying the 16c O_h sites instead of the 8a T_d sites at point (2), which contributes to an increased overpotential during the charging cycle, as discussed in Figure 5. Our DFT results in Figure 6 show that Li ions will start migrating once there is a local region of concentration that is Li-deficient. At point (3), the $I_{(113)}/I_{(004)}$ ratio reaches the highest value, indicating that the Li^+ ions in the $Fd\bar{3}m$ phase are mostly occupying the T_d sites (whereas our cathode sample contains Li^+ ions occupying the O_h sites in the $R\bar{3}m$ phase). Once the Li/LT-$LiCo_{0.9}Ni_{0.1}O_2$ cell is discharged, the ratio of $I_{(113)}/I_{(004)}$ quickly drops at point (4), suggesting that some of the T_d Li ions are also moving into the O_h sites.

Combining this experimental observation with the calculated results in Figures 5 and 6, we conclude the following: (i) The barrier for Li^+ ion migration from the O_h to T_d site during the charging cycle, i.e., when $Fd\bar{3}m$ $LiCoO_2$ (or $Li_2Co_2O_4$) is delithiated, is quite low; however, the thermodynamic driving force is not large until sufficient delithiation has occurred. (ii) Near the chemical composition of $LiCo_2O_4$ (i.e., normal spinel), Li^+ ion migration from O_h and T_d is favorable in terms of both thermodynamics and kinetics, i.e., the barrier to migrate is low and the thermodynamic driving force is large. (iii) Depending on the relative fractions of lithium ions occupying the O_h vs T_d sites at intermediate compositions, a small overpotential (~0.2 V) can occur during the charging process. (iv) During the discharge, there are sufficient O_h sites available for Li^+ ion insertion and migration (but the migration energy from T_d to O_h would be very high near the chemical composition of $LiCo_2O_4$). (v) The Li^+ ions at the T_d sites will migrate to the adjacent O_h sites as the lithiation continues and the barrier becomes low (see Figure 6a).

III.III. Exploring the Chemical Space of Li−Co−Mn−Ni−O. Overcoming the current limitations of lithium-rich cathode materials such as $xLi_2MnO_3\cdot(1-x)LiMO_2$ (M = Ni,

DOI: 10.1021/acsami.8b00394
ACS Appl. Mater. Interfaces 2018, 10, 13479−13490

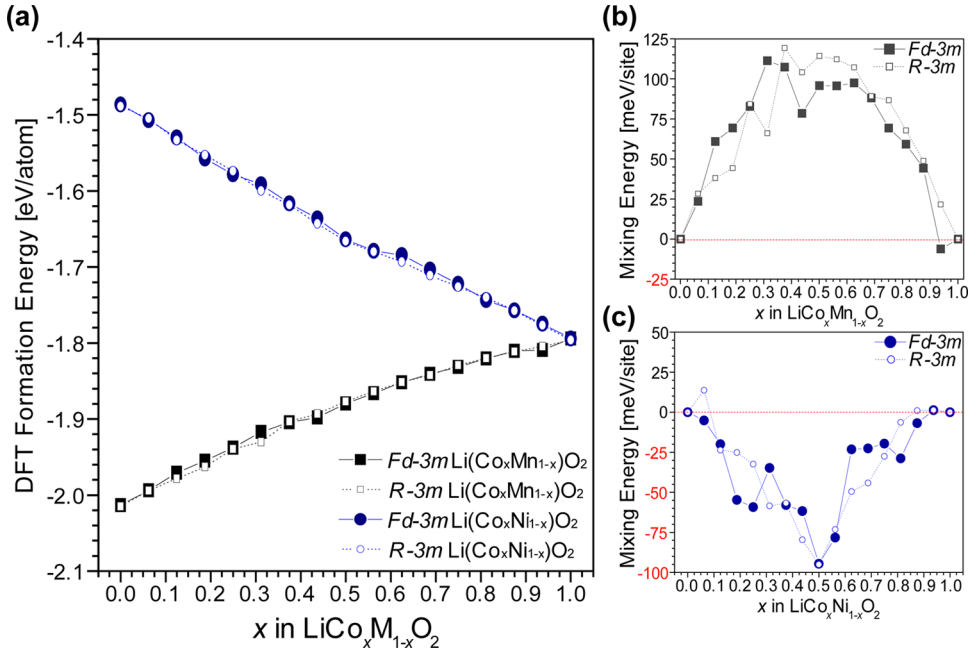

Figure 8. (a) Calculated DFT formation energies of $LiCo_xM_{1-x}O_2$ (M = Mn or Ni; $0 \le x \le 1$) in both $Fd\bar{3}m$ and $R\bar{3}m$ structures. The mixing energies of (b) Mn and (c) Ni on the Co sublattice of $LiCo_xM_{1-x}O_2$.

Co, Mn) layered−layered materials[54−60] by including a third component (spinel or overlithiated spinel)[15,16,43] is being investigated as a possible means to meet the energy density requirements for the next-generation advanced lithium-ion batteries. Over the past 2 decades, the substitution of Ni and/or Mn by Co and controlling their chemical compositions has been identified as one path to improve and optimize the electrochemical performance of electrode materials. The implementation of a practical lithium-ion cell containing the layered $LiNi_xCo_yMn_zO_2$ ($x + y + z = 1$) cathode materials has been pursued for the development of durable and affordable large-scale batteries. However, there have been few studies of the structure and energetics of possible phases in the the Li−Co−Mn/Ni−O space. For example, Bhattacharya et al.[61] studied the quaternary normal spinel oxides (AB_2O_4) using DFT and found that Co−Mn and Co−Ni ordering in the spinel structure is favored, resulting in stable $LiCoMnO_4$ and $LiCoNiO_4$ quarternary compounds. Delithiated versions of these compounds do not show an energetic tendency for cation migration (e.g., inverse spinel formation), thus making a topotactic reaction upon delithiation possible, i.e., the crystal structure remains intact upon delithiation. Another recent experimental study[62] has explored a number of metastable quaternary $Li(Ni_{1-y-z}Mn_yCo_z)_2O_4$ normal spinel compounds by a low-temperature synthesis approach. However, none of above-mentioned studies have considered the overlithiated spinel $Fd\bar{3}m$ phases.

Here, we have examined the substitution of Mn or Ni on the Co site of both cubic $Fd\bar{3}m$ and layered $R\bar{3}m$ lithium cobalt oxide structures, i.e., $Li_{16}Co_{16-x}M_xO_{32}$ (where M = Mn or Ni; $0 \le x \le 16$), sampling a wide range of compositions and exhaustively searching through all the geometric configurations at each composition (see refs 47−49 and Section S4 in the SI for further details on generating $Li_{16}Co_{16-x}M_xO_{32}$ structures, the accuracy of choosing low-energy structures from the calculated electrostatic energies in comparison to the DFT-level calculations, and their statistical validations).

Figure 8a displays the calculated ground state DFT formation energy (ΔH_f) of $LiCo_xM_{1-x}O_2$ (M = Mn or Ni; and $0 \le x \le 1$) sampled uniformly through the composition space. Here, the DFT formation energy of a generic $LiMO_2$ compound is defined as follows: $\Delta H_f\ (LiCo_xM_{1-x}O_2) = E_0(LiCo_xM_{1-x}O_2) - \mu_{Li} - x\mu_{Co} - (1-x)\mu_M - 2\mu_O$, where $E_0(LiCo_xM_{1-x}O_2)$ is the calculated DFT total energy of $LiCo_xM_{1-x}O_2$ and μ_i (i = Li, Co, M, O) is the chemical potential of component i. As discussed in the earlier sections, the energy difference between the $Fd\bar{3}m$ and $R\bar{3}m$ structures at each composition is almost negligible. Further, the calculated ΔH_f of $LiCo_xM_{1-x}O_2$ varies almost linearly between the end-members, $LiCoO_2$ and $LiMO_2$ (M = Mn or Ni) in Figure 8a.

The mixing tendency of two cathode components, here, $LiCoO_2$ and $LiMO_2$ (M = Mn or Ni), can be obtained using $\Delta E_{mix} = E_0(LiCo_xM_{1-x}O_2) - \{xE_0(LiCoO_2) + (1-x)E_0(LiMO_2)\}$, where $E_0(LiCo_xM_{1-x}O_2)$, $E_0(LiCoO_2)$, and $E_0(LiMO_2)$ are the calculated DFT total energies of either $Fd\bar{3}m$ or $R\bar{3}m$ $LiCo_xM_{1-x}O_2$, $LiCoO_2$, and $LiMO_2$ (M = Mn or Ni), respectively. A slightly negative ΔE_{mix} (i.e., −25 to 0 meV/site) indicates a weak preference for ordering, which could be overcome by configurational entropy at elevated temperatures to form a solid solution. A significantly more negative ΔE_{mix} (i.e., <−25 meV/site) usually leads to the formation of an ordered compound. In contrast, a slightly positive ΔE_{mix} (i.e., 0−25 meV/site) hints at a weak preference for phase separation; again, configurational entropy could favor solid solutions at elevated temperatures. Lastly, a significantly positive ΔE_{mix} (i.e., >25 meV/site) usually results in a two-phase miscibility gap. From Figure 8b, it can be observed that Mn substitution in either $Fd\bar{3}m$ or $R\bar{3}m$ $LiCo_xMn_{1-x}O_2$ is only favorable at dilute concentrations of Mn ($x > 0.9$). In fact, the mixing of Mn and Co on the Co sublattice in the LCO structure becomes increasingly unfavorable toward equiatomic compositions of Mn and Co. On the other hand, as seen in Figure 8c, the mixing of Ni and Co on the Co sublattice is generally favorable at all compositions. In fact, the energy of

DOI: 10.1021/acsami.8b00394
ACS Appl. Mater. Interfaces 2018, 10, 13479−13490

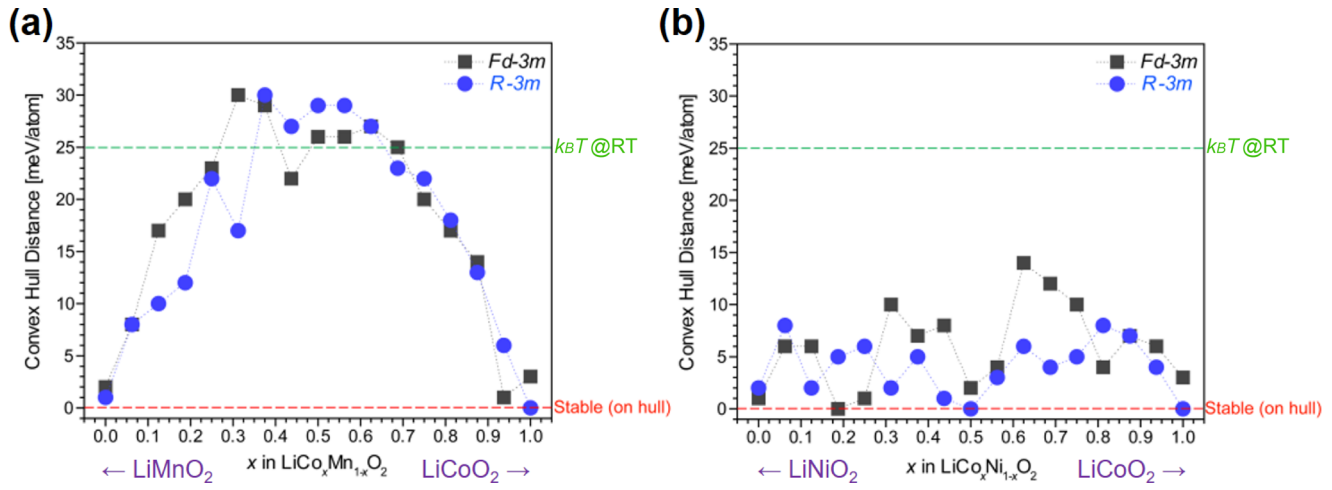

Figure 9. Convex hull analysis of $Fd\bar{3}m$ and $R\bar{3}m$ $LiCo_xM_{1-x}O_2$ ($0 \le x \le 1$) for (a) M = Mn and (b) M = Ni, where stable (i.e., on the hull) and nearly stable (i.e., within 25 meV/atom of the hull corresponding to k_BT at room temperature) compounds are identified. Please see Figure S5 in the SI for the calculated XRD pattern and crystal structure of the "stable" $LiCo_{0.1875}Ni_{0.8125}O_2$ compound, predicted in panel (b).

mixing becomes increasingly negative (up to ~−100 meV/site) toward equiatomic compositions of Ni and Co, hence compositions close to $LiCo_{0.5}Ni_{0.5}O_2$ are likely to form ordered compounds.

While the calculated ΔE_{mix} can provide new insights into the mixing between the two end-members, $LiCoO_2$ and $LiMO_2$, we further investigate the thermodynamic stabilities of $LiCo_xMn_{1-x}O_2$ against all the other known phases in the quaternary space currently in the OQMD.[39,40] Large thermodynamic databases such as the OQMD, which include the energies and phase stabilities of most currently known crystalline compounds in the ICSD and hypothetical compounds based on decorations of prototype structures,[39,40,63] have been previously used to predict new battery materials.[64−67] The metric of thermodynamic stability of a compound is given by its distance from the so-called convex hull of all the phases within the respective phase space. A compound is thermodynamically stable if it lies on the convex hull of its chemical space (i.e., a hull distance of 0 meV/atom). Strongly stable compounds are likely to be synthesizable, and those that are "nearly stable" (i.e., that lie close to the convex hull, with a hull distance of <~25 meV/atom, corresponding to k_BT at room temperature to account for the thermal effects) can be possibly synthesized experimentally.[39,40,64−67] In Figure 9, we have calculated the thermodynamic phase stability of all the $LiCo_xM_{1-x}O_2$ compounds vs all the other compounds present within the Li−Co−Mn−Ni−O chemical space (the set of thermodynamically stable compounds in this pentenary space is represented as a graph in Figure S4).

Figure 9a shows that Mn substitution on the Co sublattice can lead to nearly stable compounds for both $R\bar{3}m$ and $Fd\bar{3}m$ structures for $x < 0.3$ and $x > 0.7$ in $LiCo_xMn_{1-x}O_2$. On the other hand, in the case of $LiCo_xNi_{1-x}O_2$, all the compositions are predicted to be stable or nearly stable (within ~10−15 meV/atom of the convex hull; see Figure 9b). Further, two compounds at compositions $LiCo_{0.5}Ni_{0.5}O_2$ (layered) and $LiCo_{0.1875}Ni_{0.8125}O_2$ (spinel-based) are found to lie on the convex hull. The former, $LiCo_{0.5}Ni_{0.5}O_2$, has already been synthesized as a layered $R\bar{3}m$ structure in the experiments.[68,69] The latter lithiated spinel-based compound, $LiCo_{0.1875}Ni_{0.8125}O_2$ (having lattice parameters of $a = b = c = \sim 8.2$ Å and $\alpha = \beta = \lambda = 90°$ according to our DFT calculations; see Figure S5 in the SI), with a composition similar to that of the commercially available $R\bar{3}m$ $LiNi_{0.8}Co_{0.15}Al_{0.05}O_2$ (NCA) layered cathode materials, is hereby proposed for further experimental investigation, in addition to the previously explored $LiCo_{1-x}Ni_xO_2$ ($0 \le x \le 0.5$) system.[16]

IV. CONCLUSIONS

We used a DFT-based theoretical approach to investigate the phase stability of lithium cobalt oxide in cubic vs layered forms, and found that two phases are extremely competitive in terms of free energy. While the $R\bar{3}m$ layered $LiCoO_2$ is predicted to be the ground state structure at all the temperatures, the $Fd\bar{3}m$ cubic lithiated spinel structure is predicted to be accessible at low temperatures due to the sluggish kinetics. We have carefully examined the electrochemical performance of both $Fd\bar{3}m$ and $R\bar{3}m$ $LiCoO_2$ cathode material and further studied the kinetics of lithium migration during the charging cycle in LT-$LiCoO_2$ (or $Li_2Co_2O_4$) by calculating the migration barriers and analyzing the ex situ X-ray diffractions. Lastly, we explored the Li−Co−Mn−Ni−O chemical space to search for a new $LiCo_xM_{1-x}O_2$ (M = Mn or Ni; $0 \le x \le 1$) quaternary cathode material that can be synthesized experimentally. Our analysis shows that $Fd\bar{3}m$ $LiCo_{0.1875}Ni_{0.8125}O_2$, with a chemical composition close to that of layered $LiNi_{0.8}Co_{0.15}Al_{0.05}O_2$ (NCA), is predicted to be thermodynamically stable; many other Mn- and Ni-substituted $LiCo_xM_{1-x}O_2$ cathode materials can also be accessed experimentally (i.e., being close to the convex hull with a hull distance of <~25 meV/atom). These predicted materials may be of interest either as single cathodes or integrated within composite cathodes such as layered−layered electrodes for advanced next-generation LIB applications.

■ ASSOCIATED CONTENT

Supporting Information

The Supporting Information is available free of charge on the ACS Publications website at DOI: 10.1021/acsami.8b00394.

Stability of the $Fd\bar{3}m$ phase with Ni substitution, construction of LT-/HT-LCO interface and voltage calculations, XRD peak intensity of $I_{(113)}$ and $I_{(004)}$ in LT-LCO and $LiCo_2O_4$ spinel, structural search for new $LiCo_xM_{1-x}O_2$ compounds, a graph representation of the

DOI: 10.1021/acsami.8b00394
ACS Appl. Mater. Interfaces 2018, 10, 13479−13490

Li−Co−Mn−Ni−O convex hull, and the predicted XRD pattern of new lithiated spinel-based $LiCo_{0.1875}Ni_{0.8125}O_2$ and its crystal structure (PDF)

AUTHOR INFORMATION

Corresponding Authors

*E-mail: eungje.lee@anl.gov (E.L.).
*E-mail: c-wolverton@northwestern.edu (C.W.).

ORCID

Zhenpeng Yao: 0000-0001-8286-8257
Maximilian Amsler: 0000-0001-8350-2476
Jiangang He: 0000-0001-9643-3617
Jason R. Croy: 0000-0002-5839-3666
Chris Wolverton: 0000-0003-2248-474X

Present Addresses

[‖]Laboratory of Atomic and Solid State Physics, Cornell University, Ithaca, New York 14853, United States (M.A.).
[§]Research Laboratory of Electronics, Massachusetts Institute of Technology, 77 Massachusetts Avenue, Cambridge, Massachusetts 02139, United States (S.K.).

Notes

The authors declare no competing financial interest.

ACKNOWLEDGMENTS

S.K. (conceived and designed project details; performed all the DFT calculations) was supported by Northwestern-Argonne Institute of Science and Engineering (NAISE) and partially supported by the 2016 ECS Edward G. Weston Summer Fellowship from the Electrochemical Society (ECS). V.I.H. (new structural search and stability analysis) was supported by National Science Foundation (NSF, DMR-1309957). Z.Y. (generated prototype structures) and C.W. (planned and supervised all the aspects of the research project) were supported as part of the Center for Electrochemical Energy Science (CEES), an Energy Frontier Research Center (EFRC) funded by the U.S. Department of Energy, Office of Science, Office of Basic Energy Sciences (Award No. DE-AC02-06CH11357). Z.L. (generated interfacial structures) and S.H. (phonon calculation) were supported by the Dow Chemical Company. M.A. (generated $LiCoO_2$ polymorphs via MHM) acknowledges support from the Novartis Universität Basel Excellence Scholarship for Life Sciences and the Swiss National Science Foundation (P300P2-158407 and P300P2-174475). J.H. (collaborated on phonon calculations and performed HSE calculations) acknowledges support via ONR STTR N00014-13-P-1056. Support from the Advanced Batteries Materials Research (BMR) Program, in particular David Howell and Tien Duong, of the U.S. Department of Energy, Office of Energy Efficiency and Renewable Energy, is gratefully acknowledged by J.R.C., E.L., and M.M.T. (contributed to the main idea and to the writing of this manuscript). This research was supported in part through the computational resources and staff contributions provided for the Quest high-performance computing facility at Northwestern University, which is jointly supported by the Office of the Provost, the Office for Research, and Northwestern University Information Technology. Use of the Center for Nanoscale Materials, an Office of Science user facility, was supported by the U.S. Department of Energy, Office of Science, Office of Basic Energy Sciences, under Contract No. DE-AC02-06CH11357. Computational resources from the Swiss National Supercomputing Center in Lugano (project s700), the Extreme Science and Engineering Discovery Environment (XSEDE) (which is supported by National Science Foundation grant number OCI-1053575), the Bridges system at the Pittsburgh Supercomputing Center (PSC) (which is supported by NSF award number ACI-1445606), and the National Energy Research Scientific Computing Center (DOE: DE-AC02-05CH11231) are gratefully acknowledged. All the authors contributed to the data analysis and in writing the manuscript.

REFERENCES

(1) Gummow, R. J.; Liles, D. C.; Thackeray, M. M. Spinel Versus Layered Structures for Lithium Cobalt Oxide Synthesized at 400 °C. *Mater. Res. Bull.* **1993**, *28*, 235−246.
(2) Wolverton, C.; Zunger, A. Cation and Vacancy Ordering in Li_xCoO_2. *Phys. Rev. B: Condens. Matter Mater. Phys.* **1998**, *57*, 2242−2252.
(3) Wolverton, C.; Zunger, A. Prediction of Li Intercalation and Battery Voltages in Layered vs. Cubic Li_xCoO_2. *J. Electrochem. Soc.* **1998**, *145*, 2424−2431.
(4) Van der Ven, A.; Aydinol, M. K.; Ceder, G. First-Principles Evidence for Stage Ordering in Li_xCoO_2. *J. Electrochem. Soc.* **1998**, *145*, 2149−2155.
(5) Wolverton, C.; Zunger, A. First-Principles Prediction of Vacancy Order-Disorder and Intercalation Battery Voltages in Li_xCoO_2. *Phys. Rev. Lett.* **1998**, *81*, 606.
(6) Van der Ven, A.; Aydinol, M. K.; Ceder, G.; Kresse, G.; Hafner, J. First-principles investigation of phase stability in Li_xCoO_2. *Phys. Rev. B* **1998**, *58*, 2975.
(7) Van der Ven, A.; Ceder, G. Electrochemical properties of spinel Li_xCoO_2: A first-principles investigation. *Phys. Rev. B* **1999**, *59*, 742.
(8) Wang, H.; Jang, Y.-I.; Huang, B.; Sadoway, D. R.; Chiang, Y.-M. TEM Study of Electrochemical Cycling-Induced Damage and Disorder in $LiCoO_2$ Cathodes for Rechargeable Lithium Batteries. *J. Electrochem. Soc.* **1999**, *146*, 473−480.
(9) Gabrisch, H.; Yazami, R.; Fultz, B. Hexagonal to cubic spinel transformation in lithiated cobalt oxide TEM Investigation. *J. Electrochem. Soc.* **2004**, *151*, A891−A897.
(10) Choi, S.; Manthiram, A. Synthesis and Electrochemical Properties of $LiCo_2O_4$ Spinel Cathodes. *J. Electrochem. Soc.* **2002**, *149*, A162−A166.
(11) Gummow, R. J.; Thackeray, M. M.; David, W. I. F.; Hull, S. Structure and Electrochemistry of Lithium Cobalt Oxide Synthesized at 400 °C. *Mater. Res. Bull.* **1992**, *27*, 327−337.
(12) Gummow, R. J.; Thackeray, M. M. Lithium Cobalt Nickel-Oxide Cathode Materials Prepared at 400 °C for Rechargeable Lithium Batteries. *Solid State Ionics* **1992**, *53*−*56*, 681−687.
(13) Rossen, E.; Reimers, J. N.; Dahn, J. R. Synthesis and Electrochemistry of Spinel LT-$LiCoO_2$. *Solid State Ionics* **1993**, *62*, 53−60.
(14) Aykol, M.; Kim, S.; Wolverton, C. van der Waals Interactions in Layered Lithium Cobalt Oxides. *J. Phys. Chem. C* **2015**, *119*, 19053−19058.
(15) Long, B. R.; Croy, J. R.; Park, J. S.; Wen, J.; Miller, D. J.; Thackeray, M. M. Advances in Stabilizing 'Layered-Layered' $xLi_2MnO_3{\cdot}(1\text{-}x)LiMO_2$ (M = Mn, Ni, Co) Electrodes with a Spinel Component. *J. Electrochem. Soc.* **2014**, *161*, A2160−A2167.
(16) Lee, E.; Blauwkamp, J.; Castro, F. C.; Wu, J.; Dravid, V. P.; Yan, P.; Wang, C.; Kim, S.; Wolverton, C.; Benedek, R.; Dogan, F.; Park, J. S.; Croy, J. R.; Thackeray, M. M. Exploring Lithium-Cobalt-Nickel Oxide Spinel Electrodes for ≥3.5 V Li-Ion Cells. *ACS Appl. Mater. Interfaces* **2016**, *8*, 27720−27729.
(17) Kresse, G.; Hafner, J. Ab Initio Molecular Dynamics for Liquid Metals. *Phys. Rev. B: Condens. Matter Mater. Phys.* **1993**, *47*, 558.
(18) Kresse, G.; Furthmüller, J. Efficiency of Ab-initio Total Energy Calculations for Metals and Semiconductors Using a Plane-wave Basis Set. *Comput. Mater. Sci.* **1996**, *6*, 15−50.

DOI: 10.1021/acsami.8b00394
ACS Appl. Mater. Interfaces 2018, 10, 13479−13490

(19) Kresse, G.; Joubert, D. From Ultrasoft Pseudopotentials to the Projector Augmented-wave Method. *Phys. Rev. B: Condens. Matter Mater. Phys.* **1999**, *59*, 1758.
(20) Dudarev, S. L.; Botton, G. A.; Savrasov, S. Y.; Humphreys, C. J.; Sutton, A. P. Electron-energy-loss spectra and the structural stability of nickel oxide: An LSDA + U study. *Phys. Rev. B* **1998**, *57*, 1505.
(21) Heyd, J.; Scuseria, G. E.; Ernzerhof, M. Hybrid functionals based on a screened Coulomb potential. *J. Chem. Phys.* **2003**, *118*, 8207–8215.
(22) Heyd, J.; Scuseria, G. E.; Ernzerhof, M. Erratum: "Hybrid functionals based on a screened Coulomb potential" [J. Chem. Phys. 118, 8207 (2003)]. *J. Chem. Phys.* **2006**, *124*, No. 219906.
(23) Momma, K.; Izumi, F. VESTA 3 for three-dimensional visualization of crystal, volumetric and morphology data. *J. Appl. Crystallogr.* **2011**, *44*, 1272–1276.
(24) Goedecker, S. Minima hopping: An efficient search method for the global minimum of the potential energy surface of complex molecular systems. *J. Chem. Phys.* **2004**, *120*, 9911–9917.
(25) Amsler, M.; Goedecker, S. Crystal structure prediction using the minima hopping method. *J. Chem. Phys.* **2010**, *133*, No. 224104.
(26) Amsler, M.; Flores-Livas, J. A.; Lehtovaara, L.; Balima, F.; Ghasemi, S. A.; Machon, D.; Pailhès, S.; Willand, A.; Caliste, D.; Botti, S.; Miguel, A. S.; Goedecker, S.; Marques, M. A. L. Crystal structure of cold compressed graphite. *Phys. Rev. Lett.* **2012**, *108*, No. 065501.
(27) Amsler, M.; Flores-Livas, J. A.; Huan, T. D.; Botti, S.; Marques, M. A. L.; Goedecker, S. Novel Structural Motifs in Low Energy Phases of $LiAlH_4$. *Phys. Rev. Lett.* **2012**, *108*, No. 205505.
(28) Tian, Y.; Jia, S.; Cava, R. J.; Zhong, R.; Schneeloch, J.; Gu, G.; Burch, K. S. Understanding the evolution of anomalous anharmonicity in $Bi_2Te_{3-x}Se_x$. *Phys. Rev. B* **2017**, *95*, No. 094104.
(29) Huan, T. D.; Amsler, M.; Tuoc, V. N.; Willand, A.; Goedecker, S. Low-energy structures of zinc borohydride $Zn(BH_4)_2$. *Phys. Rev. B* **2012**, *86*, No. 224110.
(30) Roy, S.; Goedecker, S.; Hellmann, V. Bell-Evans-Polanyi principle for molecular dynamics trajectories and its implications for global optimization. *Phys. Rev. E* **2008**, *77*, No. 056707.
(31) Sicher, M.; Mohr, S.; Goedecker, S. Efficient moves for global geometry optimization methods and their application to binary systems. *J. Chem. Phys.* **2011**, *134*, No. 044106.
(32) Togo, A.; Tanaka, I. First principles phonon calculations in materials science. *Scr. Mater.* **2015**, *108*, 1–5.
(33) Michel, K. J.; Wolverton, C. Symmetry building Monte Carlo-based crystal structure prediction. *Comput. Phys. Commun.* **2014**, *185*, 1389–1393.
(34) Henkelman, G.; Uberuaga, B. P.; Jónsson, H. A climbing image nudged elastic band method for finding saddle points and minimum energy paths. *J. Chem. Phys.* **2000**, *113*, 9901–9904.
(35) Henkelman, G.; Jónsson, H. Improved tangent estimate in the nudged elastic band method for finding minimum energy paths and saddle points. *J. Chem. Phys.* **2000**, *113*, 9978–9985.
(36) Hart, G. L. W.; Forcade, R. W. Algorithm for generating derivative structures. *Phys. Rev. B* **2008**, *77*, No. 224115.
(37) Hart, G. L. W.; Forcade, R. W. Generating derivative structures from multilattices: Algorithm and application to hcp alloys. *Phys. Rev. B* **2009**, *80*, No. 014120.
(38) Hart, G. L. W.; Nelson, L. J.; Forcade, R. W. Generating derivative structures at a fixed concentration. *Comput. Mater. Sci.* **2012**, *59*, 101–107.
(39) Saal, J. E.; Kirklin, S.; Aykol, M.; Meredig, B.; Wolverton, C. Materials Design and Discovery with High-Throughput Density Functional Theory: The Open Quantum Materials Database (OQMD). *JOM* **2013**, *65*, 1501–1509.
(40) Kirklin, S.; Saal, J. E.; Meredig, B.; Thompson, A.; Doak, J. W.; Aykol, M.; Rühl, S.; Wolverton, C. The Open Quantum Materials Database (OQMD): assessing the accuracy of DFT formation energies. *npj Comput. Mater.* **2015**, *1*, No. 15010.
(41) Klimeš, J.; Bowler, D. R.; Michaelides, A. Chemical Accuracy for the van der Waals Density Functional. *J. Phys.: Condens. Matter* **2010**, *22*, No. 022201.
(42) Klimeš, J.; Bowler, D. R.; Michaelides, A. Van der Waals Density Functionals Applied to Solids. *Phys. Rev. B: Condens. Matter Mater. Phys.* **2011**, *83*, No. 195131.
(43) Kim, S.; Noh, J.-K.; Aykol, M.; Lu, Z.; Kim, H.; Choi, W.; Kim, C.; Chung, K. Y.; Wolverton, C.; Cho, B.-W. Layered-Layered-Spinel Cathode Materials Prepared by a High-Energy Ball-Milling Process for Lithium-ion Batteries. *ACS Appl. Mater. Interfaces* **2016**, *8*, 363–370.
(44) Shao-Horn, Y.; Hackney, S. A.; Kahaian, A. J.; Thackeray, M. M. Structural Stability of $LiCoO_2$ at 400 °C. *J. Solid State Chem.* **2002**, *168*, 60–68.
(45) Wolverton, C.; Ozoliņš, V. Entropically favored ordering: the metallurgy of Al_2Cu revisited. *Phys. Rev. Lett.* **2001**, 5518–5521.
(46) Amatucci, G. G.; Tarascon, J. M.; Klein, L. C. CoO_2, the end member of the $LiCoO_2$ solid solution. *J. Electrochem. Soc.* **1996**, *143*, 1114–1123.
(47) Yao, Z.; Kim, S.; Aykol, M.; Li, Q.; Wu, J.; He, J.; Wolverton, C. Revealing the conversion mechanism of transition metal oxide electrodes during lithiation from first-principles. *Chem. Mater.* **2017**, *29*, 9011–9022.
(48) Li, Q.; Liu, H.; Yao, Z.; Cheng, J.; Li, T.; Li, Y.; Wolverton, C.; Wu, J.; Dravid, V. P. Electrochemistry of Selenium with Sodium and Lithium: Kinetics and Reaction Mechanism. *ACS Nano* **2016**, *10*, 8788–8795.
(49) Li, Q.; Yao, Z.; Wu, Z.; Mitra, S.; Hao, S.; Sahuc, T. S.; Li, Y.; Wolverton, C.; Dravid, V. P. Intermediate phases in sodium intercalation into MoS_2 nanosheets and their implications for sodium-ion batteries. *Nano Energy* **2017**, *38*, 342–349.
(50) Orikasa, Y.; Maeda, T.; Koyama, Y.; Murayama, H.; Fukuda, K.; Tanida, H.; Arai, H.; Matsubara, E.; Uchimoto, Y.; Ogumi, Z. Direct Observation of a Metastable Crystal Phase of Li_xFePO_4 under Electrochemical Phase Transition. *J. Am. Chem. Soc.* **2013**, *135*, 5497–5500.
(51) Shin, E. J.; Kim, S.; Noh, J.-K.; Byun, D.; Chung, K. Y.; Kim, H. S.; Cho, B.-W. A Green Recycling Process Designed for $LiFePO_4$ Cathode Materials for Li-ion Batteries. *J. Mater. Chem. A* **2015**, *3*, 11493–11502.
(52) Choi, S.; Manthiram, A. Synthesis and Electrode Properties of Metastable $Li_2Mn_4O_{9-\delta}$ Spinel Oxides. *J. Electrochem. Soc.* **2000**, *147*, 1623–1629.
(53) Bhattacharya, J.; Wolverton, C. Relative stability of normal vs. inverse spinel for 3d transition metal oxides as lithium intercalation cathodes. *Phys. Chem. Chem. Phys.* **2013**, *15*, 6486–6498.
(54) Thackeray, M. M.; Wolverton, C.; Isaacs, E. D. Electrical energy storage for transportation—approaching the limits of, and going beyond, lithium-ion batteries. *Energy Environ. Sci.* **2012**, *5*, 7854–7863.
(55) Thackeray, M. M.; Kang, S.-H.; Johnson, C. S.; Vaughey, J. T.; Benedek, R.; Hackney, S. A. Li_2MnO_3-stabilized $LiMO_2$ (M = Mn, Ni, Co) Electrodes for Lithium-ion Batteries. *J. Mater. Chem.* **2007**, *17*, 3112–3125.
(56) Kim, S.; Kim, C.; Noh, J.-K.; Yu, S.; Kim, S.-J.; Chang, W.; Choi, W. C.; Chung, K. Y.; Cho, B.-W. Synthesis of Layered-layered $xLi_2MnO_3 \cdot (1-x)LiMO_2$ (M = Mn, Ni, Co) Nanocomposite Electrodes Materials by Mechanochemical Process. *J. Power Sources* **2012**, *220*, 422–429.
(57) Noh, J.-K.; Kim, S.; Kim, H.; Choi, W.; Chang, W.; Byun, D.; Cho, B.-W.; Chung, K. Y. Mechanochemical Synthesis of Li_2MnO_3 Shell/$LiMO_2$ (M = Ni, Co, Mn) Core-Structured Nanocomposites for Lithium-Ion Batteries. *Sci. Rep.* **2014**, *4*, No. 4847.
(58) Croy, J. R.; Iddir, H.; Gallagher, K.; Johnson, C. S.; Benedek, R.; Balasubramanian, M. First-charge instabilities of layered-layered lithium-ion-battery materials. *Phys. Chem. Chem. Phys.* **2015**, *17*, 24382–24391.
(59) Croy, J. R.; Balasubramanian, M.; Gallagher, K. G.; Burrell, A. K. Review of the U.S. Department of Energy's "Deep Dive" effort to understand voltage fade in Li- and Mn-rich cathodes. *Acc. Chem. Res.* **2015**, *48*, 2813–2821.
(60) Croy, J. R.; Gallagher, K. G.; Balasubramanian, M.; Chen, Z.; Ren, Y.; Kim, D.; Kang, S.-H.; Dees, D. W.; Thackeray, M. M.

DOI: 10.1021/acsami.8b00394
ACS Appl. Mater. Interfaces 2018, 10, 13479–13490

Examining hysteresis in composite $xLi_2MnO_3\bullet(1\text{-}x)LiMO_2$ cathode structures. *J. Phys. Chem. C* **2013**, *117*, 6525−6536.
(61) Bhattacharya, J.; Wolverton, C. Prediction of Quaternary Spinel Oxides as Li-Battery Cathodes: Cation Site Preference, Metal Mixing, Voltage and Phase Stability. *J. Electrochem. Soc.* **2014**, *161*, A1440−A1446.
(62) Kan, W. H.; Huq, A.; Manthiram, A. Exploration of a Metastable Normal Spinel Phase Diagram for the Quaternary Li−Ni−Mn−Co−O System. *Chem. Mater.* **2016**, *28*, 1832−1837.
(63) Jain, A.; Ong, S. P.; Hautier, G.; Chen, W.; Richards, W. D.; Dacek, S.; Cholia, S.; Gunter, D.; Skinner, D.; Ceder, G.; Persson, K. A. Commentary: The Materials Project: A materials genome approach to accelerating materials innovation. *APL Mater.* **2013**, *1*, No. 011002.
(64) Kirklin, S.; Meredig, B.; Wolverton, C. High-Throughput Computational Screening of New Li-Ion Battery Anode Materials. *Adv. Energy Mater.* **2013**, *3*, 252−262.
(65) Kim, S.; Aykol, M.; Hegde, V. I.; Lu, Z.; Kirklin, S.; Croy, J. R.; Thackeray, M. M.; Wolverton, C. Material design of high-capacity Li-rich layered-oxide electrodes: Li_2MnO_3 and beyond. *Energy Environ. Sci.* **2017**, *10*, 2201−2211.
(66) Aykol, M.; Kirklin, S.; Wolverton, C. Thermodynamic Aspects of Cathode Coatings for Lithium-Ion Batteries. *Adv. Energy Mater.* **2014**, *4*, No. 1400690.
(67) Aykol, M.; Kim, S.; Hegde, V. I.; Snydacker, D.; Lu, Z.; Hao, S.; Kirklin, S.; Morgan, D.; Wolverton, C. High-throughput computational design of cathode coatings for Li-ion batteries. *Nat. Commun.* **2016**, *7*, No. 13779.
(68) Reddy, M. V.; Subba Rao, G. V.; Chowdari, B. V. R. Preparation and Characterization of $LiNi_{0.5}Co_{0.5}O_2$ and $LiNi_{0.5}Co_{0.4}Al_{0.1}O_2$ by Molten Salt Synthesis for Li Ion Batteries. *J. Phys. Chem. C* **2007**, *111*, 11712−11720.
(69) Montoro, L.; Abbate, M.; Almeida, E.; Rosolen, J. Electronic structure of the transition metal ions in $LiCoO_2$, $LiNiO_2$ and $LiCo_{0.5}Ni_{0.5}O_2$. *Chem. Phys. Lett.* **1999**, *309*, 14−18.

DOI: 10.1021/acsami.8b00394
ACS Appl. Mater. Interfaces 2018, 10, 13479−13490